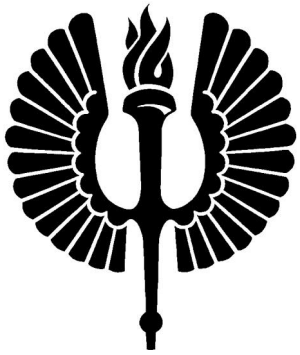

ELECTRONIC STRUCTURE OF METAL ENCAPSULATING DELTAHEDRAL GERMANIUM CLUSTERS

Petteri Vainikka

Master's Thesis
December 2018

DEPARTMENT OF CHEMISTRY
UNIVERSITY OF TURKU
PHYSICAL AND THEORETICAL CHEMISTRY LABORATORY
UNIVERSITY OF OXFORD

There is nothing more practical than a good theory.

L. Boltzmann

VAINIKKA, PETTERI:
Electronic structure of metal encapsulating deltahedral germanium clusters.

SUPERVISORS:
Prof. John McGrady, University of Oxford
Prof. Jukka Lukkari, University of Turku
Dr. Henri Kivelä, University of Turku

Master's thesis, 35 pages.
Chemistry
December 2018

The last century has seen the dawn of a new era of research focused on Zintl phases and ions. Many of their properties have been successfully characterized, and new avenues of research are continuously explored. This work focuses on the electronic structures of two Zintl ion systems, both discovered, synthesized, and published by Dr. J. M. Goicoechea and Prof. S. C. Sevov in 2005. The first system type consists of deltahedral germanium clusters with an interstitial nickel atom, and a capping fragment consisting of a nickel atom and a ligand. The second compound consists of a similar clusters, but in a dimeric form.

The work presented here gives new insights to the electronic structure of these systems. Certain systematic changes in stability and electronic interactions were observed based on the series of density functional theory calculations performed, demonstrating that the overall electronic structure is probably complex enough to contain factors which are not accounted for by Wade's rules.

Further discoveries were made by utilizing RAS-SCF calculations. These calculations demonstrated that the nickel filament present in the second type of compounds is actively contributing to the total electron density on the cluster.

Keywords: Computational chemistry, deltahedral germanium clusters, density functional theory, post-Hartree-Fock methods.

The originality of this thesis has been checked in accordance with the University of Turku quality assurance system using the Turnitin OriginalityCheck service.

Contents

1 Introduction

Within the past century, Zintl ions have gone from being mere chemical curiosities to the forefront of research in inorganic chemistry. They are polyatomic clusters with a negative charge, composed of main group metallic and metalloidic elements, such as the one given as an example in Figure 1 below. As described later in this section with more detail, the work done in the past century has shown how these clusters can be, among other things, functionalized [1], cojoined in to a variety of larger units such as dimers and trimers via oxidative coupling [2], and endohedrally filled with transition metal atoms [3].

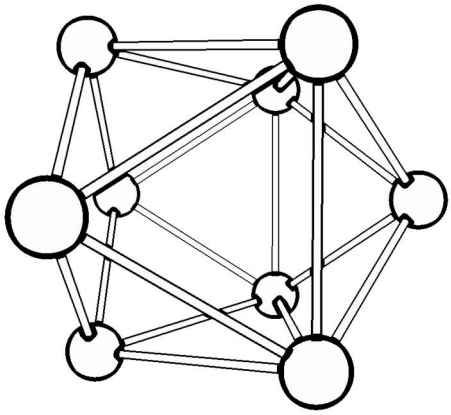

Figure 1: A nine-atom deltahedral cluster composed of a germanium atoms, $[Ge_9]^{4-}$. This work is focused on systems with a similar Ge structure with the general form $[Ni@(Ge_9Ni-L)]^{n-}$, where L is some ligand and n varies from 2 to 4. Further details are given in Section 3.

The earliest documented studies regarding the chemistry of Zintl ions and Zintl phases[1] are from the late 1800's. In a paper published in *Comptes rendus de l'Académie des Sciences* in 1891, Jacques Joannis described, for the first time, the reactions of sodium with lead and antimony in liquid ammonia, which led to green and dark red solutions. [4, 5] These discoveries were later complemented by the works of Peck, Smyth, Kraus and Zintl. [5] Although it took years of effort from multiple scientists, it was Eduard Zintl and his coworkers who managed to determine the true nature of the colourful solutions Joannis had created. In a series of papers published in 1931, 1932, and 1933 they presented their findings: The green and dark red solutions Joannis had discovered contained $[Pb_9]^{4-}$ and $[Sb_7]^{3-}$ anions, which Zintl had determined using potentiometric titration. The work presented in

[1] Compounds consisting of group 1 or 2 metals and p-block metals or metalloids.

these publications also determined the presence and composition of $[Sn_9]^{4-}$ and $[As_7]^{3-}$. [5, 6] In honour of Zintl's work with polyatomic anions, these clusters were posthumously named as Zintl ions, and their salt-like intermetallic counterparts as Zintl phases.

Up until quite recently, the consensus among chemists was that Zintl phases and Zintl ions should be considered in separate categories, with distinct properties and structures. [1, 6] This changed in 1997 when Queneau and Sevov managed to synthesize and characterize Cs_4Ge_9 and Rb_4Ge_9, both being Zintl phases which contain a previously known deltahedral Zintl ion Ge_9^{4-}. [1, 7] At the time the link between Zintl ions and phases had been established, the number of publications related to Zintl ions and phases started to grow, and the focus of scientists begun to shift more towards Zintl ions and their properties, as is evident from Figure 2 below, which compares the amount of papers published with keywords *'Zintl ion'* and *'Zintl phase'*.

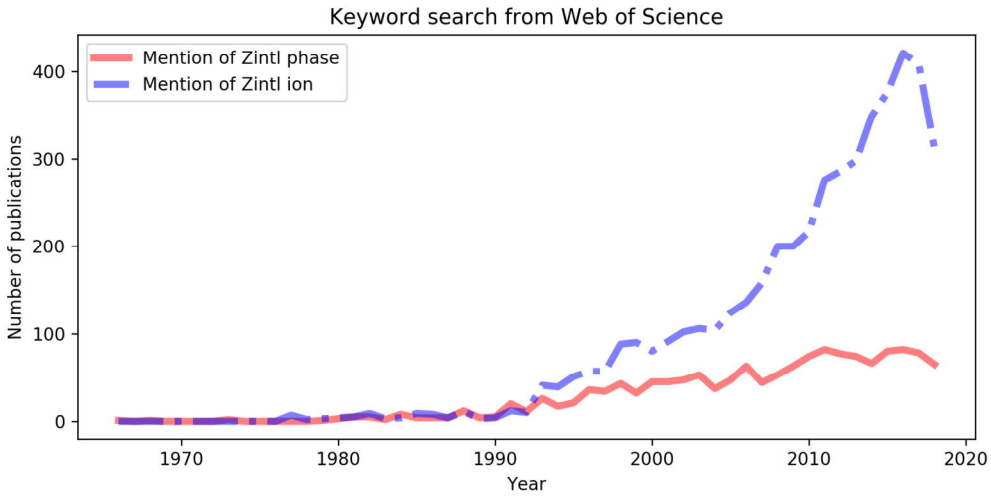

Figure 2: Number of publications containing keywords 'Zintl ion' and 'Zintl phase' as a function of time. There is a remarkable surge in number of publications during the 1990s, presumably due to the discoveries made by Queneau and Sevov. Note that each paper containing the related keyword is included, meaning that not all of the publications necessarily focus solely on Zintl ions or phases.

A second reason for the sudden sharp increase in interest towards Zintl ions can be explained with the discoveries made in the 1990s and early 2000s, which illuminated the relatively unexplored redox chemistry of Zintl ions. Contrary to the previously held belief that the highly reduced Zintl ions would disintegrate if oxidized, Gardner *et al.*, Downie *et al.*, Sevov, and

Ugrinov showed in their work how naked germanide Zintl clusters (Ge_9^{n-}, $n = 2$, 3 or 4) can be functionalized [8], coupled in to dimers [2], trimers [9], tetramers [10], or chains of infinite length [11]. These works demonstrated two important and previously unproven properties of Zintl clusters: Firstly, the clusters are able to form *exo*-bonds, and therefore it is possible to add substituents to them. Secondly, differently charged clusters are able to co-exist in an equilibrium with solvated electrons, an example being: $[Ge_9]^{4-} \leftrightharpoons [Ge_9]^{3-} + e^- \leftrightharpoons [Ge_9]^{2-} + 2e^-$. [6]

Although many of the questions that have perplexed scientists studying Zintl ions and phases through the past century have now been answered, some still remain at least partially unresolved. One such area of uncertainty is the electronic structure of some Zintl clusters which is often inferred from the crystallographic shape of the cluster using Wade's rules. [5] The work presented in this thesis aims to further describe and analyze the electronic structure of deltahedral germanium clusters with modern computational methods, and to diminish some of the uncertainties surrounding the electronic structure of these particular clusters. The thesis is structured in the following way: The first section after the introduction gives a brief and partial description of some of the computational methods used, as well as some information about the theory behind these methods. The third section describes the nature of the compounds studied and gives further details on how the computational tools were utilized. The final section focuses on inferring the results and aggregating our findings in to a set of conclusions.

2 Theory

2.1 Computational Chemistry in General

In the most general sense computational chemistry refers to a set of computer aided mathematical methods used for extracting physical and chemical information from a system [12]. These methods are widely used in almost every field of modern chemistry and they seem to have consolidated their presence in the chemical industry, especially in the pharmaceutical and materials sector.

The methods used in computational chemistry can be divided in to different groups, based on the theories they utilize. Classical methods, such as molecular mechanics and molecular dynamics use empirically derived parameters and do not have explicit treatment for electrons, thus making multiple

approximations which decreases the accuracy of these methods. The benefit is that they enable the study of systems with a large number of particles over a significant period of time (from a computational perspective). Classical methods are therefore often employed in cases where the sheer number of particles would make more accurate methods unfeasible due to lack of computational power, or in cases where employing a more sophisticated method would only yield a minor improvement in accuracy.

Non-classical methods, which in the context of this document refer to *ab-initio* and density functional theory methods, are based on quantum mechanics and treat electrons as explicit components of the system. Although both methods often make use of approximations, such as the Born-Oppenheimer approximation, their overall accuracy is significantly greater than their classical counterparts. These methods are often computationally expensive and therefore they cannot be utilized in the study of large systems or dynamic processes beyond the picosecond scale.

The treatment in this section is based on the following references: [13] [14] [15] [16] [17] [18].

2.2 Hartree-Fock SCF Method

The quantum mechanical treatment of a system relies on a set of postulates, one of which states that any and all information regarding a quantum state of a particle is contained in its wave function (Ψ). This information can be obtained by operating on the wave function with a suitable operator, which represents the observable of interest. One of the most important operators is known as the *Hamiltonian* operator ($\hat{H}$), which, when operated on the wave function, yields the Schrödinger equation from which the allowed total energies and the corresponding energy eigenstates of the system can be obtained, as is presented in Equation 1 below. It should be noted that there are no exact solutions to Eq. 1 if the described system is comprised of more than two particles.

$$\hat{H}\Psi = E\Psi \tag{1}$$

Analogously to the classical treatment of total energy, the Hamiltonian operator sums terms for both the kinetic and the potential energy components, as shown in Equation 2 below. The difference between the treatment presented in Eq. 2 and classical mechanics is found in the first two terms on the r.h.s, which are kinetic energy operators $\hat{T} = -(\hbar^2/2m)\nabla^2$ (as opposed to $p^2/2m$).

$$\hat{H} = -\sum_i \frac{\hbar^2}{2m_e}\nabla_i^2 - \sum_k \frac{\hbar^2}{2m_k}\nabla_k^2 - \sum_i \sum_k \frac{e^2 Z_k}{4\pi\epsilon_0 r_{ik}} + \sum_{k<l} \frac{e^2 Z_k Z_l}{4\pi\epsilon_0 r_{kl}} + \sum_{i<j} \frac{e^2}{4\pi\epsilon_0 r_{ij}} \tag{2}$$

In Equation 2, the first two terms on the r.h.s describe the kinetic energy of electrons and nuclei, the third term is an attractive potential between the nuclei and electrons, the fourth term is a repulsion between the nuclei, and the final term stems from electron-electron repulsion. Indices i and j count over the number of electrons present in the system, k and l do the same for nuclei. The constant e is the elementary charge, Z is the number of protons in each nuclei, ϵ_0 stands for the permittivity of vacuum, $\hbar$ is defined as $h/2\pi$, and the Laplace operator ∇^2 is defined in Equation 3 below.

$$\nabla_i^2 f = \frac{\partial^2 f}{\partial x_i^2} + \frac{\partial^2 f}{\partial y_i^2} + \frac{\partial^2 f}{\partial z_i^2} \tag{3}$$

Equation 2 can be simplified by separating the terms based on nuclear coordinates from the terms based on electronic coordinates. This is known as the Born-Oppenheimer approximation. The rationalization for this approximation emerges from the fact that nuclei are significantly heavier and slower when compared to electrons. One can quite safely assume that in the time it takes for nuclei to assume new positions in space, electrons have already 'relaxed' in to their new states around the new nuclear coordinates. An often heard macroscopic analogy is that of trying to avoid a swarm of mosquitoes by shaking ones head - by the time the comparatively massive head is moved to a new position, the swarm has already 'relaxed' to its new position around the head.

The Born-Oppenheimer approximation sets the nuclear kinetic energy component to zero (during the evaluation), thus fixing the nuclei in to a set of coordinates. The attractive potential between electrons and nuclei is now only parametrically dependent on the nuclear coordinates, and the nuclear-nuclear repulsion term becomes a constant, shifting the eigenvalues. Using this approximation, Equation 2 can now be written as follows.

$$\hat{H}_{elec} = -\sum_i \frac{\hbar^2}{2m_e}\nabla_i^2 - \sum_i \sum_k \frac{e^2 Z_k}{4\pi\epsilon_0 r_{ik}} + \sum_{i<j} \frac{e^2}{4\pi\epsilon_0 r_{ij}} \tag{4}$$

In the equation above, $\hat{H}_{elec}$ is the so-called 'electronic Hamiltonian'. The rest of the terms and variables remain unchanged and represent the same

quantities as they did in Eq. 2.

In order to apply any of the equations presented above to a chemical system, an orthonormal set of molecular wave functions needs to be acquired. One way of obtaining these wave functions is through the *variational principle*. The use of this principle starts with an assumption that an unspecified function, Φ, can be operated on by the Hamiltonian operator, and can be expanded as a linear combination of eigenfunctions of the Hamiltonian operator, as presented in Equation 5.

$$\Phi = \sum_i c_i \psi_i \tag{5}$$

If Φ is assumed to be normalized, Equation 6 follows.

$$\int \Phi^2 d\mathbf{r} = \int \sum_i c_i \psi_i \sum_j c_j \psi_j \; d\mathbf{r} = 1 \qquad c, \psi \in \Re \tag{6}$$

Reordering Equation 6 by moving the sum of coefficients c_i and c_j out of the integral, and by noting the orthonormality of both ψ_i and ψ_j, the r.h.s of Equation 6 can be simplified.

$$\int \Phi^2 d\mathbf{r} = \sum_{ij} c_i c_j \int \psi_i \psi_j \; d\mathbf{r} = \sum_{ij} c_i c_j \delta_{ij} \tag{7}$$

Due to orthonormality, the r.h.s of Equation 7 has a non-zero solution only if $i = j$, and can therefore be simplified as is shown below.

$$\int \Phi^2 d\mathbf{r} = \sum_i c_i^2 \tag{8}$$

Extracting information about the energy of the system can be achieved by applying the Hamiltonian operator to Equation 6, as shown in Equation 9 below.

$$\int \Phi \hat{H} \Phi \; d\mathbf{r} = \int \left(\sum_i c_i \psi_i \right) \hat{H} \left(\sum_j c_j \psi_j \right) \; d\mathbf{r} \tag{9}$$

By using the same logic as in Eqs. 5-8, and by noting that $\langle \Psi_i | \, \hat{H} \, | \Psi_j \rangle = E_i \delta_{ij}$, Equation 9 can be simplified in to the following form.

$$\int \Phi \hat{H} \Phi \; d\mathbf{r} = \sum_i c_i^2 E_i \tag{10}$$

From Equation 10 it is possible to see that each coefficient c_i has an associated scalar value for energy, E_i, where all the values of E_i form a set bounded from below, with the minimum value corresponding to the ground energy of the system, E_0. Assuming that the coefficients c_i have real values ($c_i \in \Re$) it is possible to form the inequality presented in Equation 11 based on the results from Eqs. 8 and 10.

$$\int \Phi \hat{H} \Phi \; d\mathbf{r} - E_0 \int \Phi^2 \; d\mathbf{r} \geq 0 \tag{11}$$

Through the manipulation presented in Equations 12 through 14, it is possible to show that the initial arbitrary wave function can be guessed, and the associated energy of this trial function can be evaluated by comparing it to the ground-state energy E_0.

$$\int \Phi \hat{H} \Phi \; d\mathbf{r} - E_0 \int \Phi^2 \; d\mathbf{r} = \sum_i c_i^2 E_i - E_0 \Big(\sum_i c_i^2 \Big) \geq 0 \tag{12}$$

$$\frac{\sum_i c_i^2 E_i}{\sum_i c_i^2} \geq E_0 \tag{13}$$

$$\frac{\int \Phi \hat{H} \Phi \; d\mathbf{r}}{\int \Phi^2 d\mathbf{r}} \geq E_0 \tag{14}$$

One sensible guess for set of trial functions can be obtained from hydrogenic atomic orbitals, which can be procured by solving Equation 4 for a system comprised of a single nucleus and an electron. A trial function (ϕ) can then be constructed by taking a linear combination of these functions, as is shown in Equation 15 below.

$$\phi = \sum_{i=1}^{N} a_i \varphi_i \tag{15}$$

The method of using atomic orbitals as a basis set (a set of functions which make up the wave function) is known as the 'LCAO-basis set method', where the abbreviation LCAO stands for 'Linear Combination of Atomic Orbitals'. These are mentioned mainly for historical reasons, as they are quite inaccurate when compared to more recently developed basis sets.

Energy of the trial function can now be evaluated in the following way, by using the variational principle and the basis set defined in Eq. 15.

$$E = \frac{\langle\phi|\,\hat{H}\,|\phi\rangle}{\langle\phi\mid\phi\rangle} = \frac{\int\left(\sum_i a_i\varphi_i\right)\hat{H}\left(\sum_j a_j\varphi_j\right)\,d\mathbf{r}}{\int\left(\sum_i a_i\varphi_i\right)\left(\sum_j a_j\varphi_j\right)\,d\mathbf{r}} = \frac{\sum_{ij} a_i a_j H_{ij}}{\sum_{ij} a_i a_j S_{ij}} \tag{16}$$

In Equation 16, S_{ij} is the so-called overlap integral, and H_{ij} is the resonance integral. The overlap integral describes the amount of overlapping between two basis functions when their phases are matched. H_{ij} has no direct physical interpretation, expect for the special case of H_{ii}, where it can be thought as the ionization potential of a single electron in an atomic orbital described by a basis function i. Equation 16 needs to be minimized in order to obtain reasonable values (assuming that the lowest possible value for energy gives the most accurate description of the system). This is done through partial derivation in relation to the coefficients a_i, and by setting $\partial E/\partial a_k = 0$. This treatment yields a set of secular equations, as shown below.

$$\sum_i^N a_i(H_{ki} - ES_{ki}) = 0 \quad \forall k \tag{17}$$

As can be seen from Equation 17, the coefficients a_i have a non-zero solution only if $H_{ki} - ES_{ki} = 0$ for every k. This can be verified by representing the set of N equations from Equation 17 in a matrix, and evaluating the so-called secular determinant, shown below.

$$\begin{vmatrix} H_{11} - ES_{11} & H_{12} - ES_{12} & \dots & H_{1N} - ES_{1N} \\ H_{21} - ES_{21} & H_{22} - ES_{22} & \dots & H_{2N} - ES_{2N} \\ \vdots & \vdots & \ddots & \vdots \\ H_{N1} - ES_{N1} & H_{N2} - ES_{N2} & \dots & H_{NN} - ES_{NN} \end{vmatrix} = |H_{ij} - ES_{ij}| = 0 \tag{18}$$

The result of this treatment is a set of N values for energy (E_j). By selecting the lowest E_j and solving the coefficients present in Equation 17, an optimal wave function, ϕ_j, is obtained. This is expressed in Equation 19 below.

$$\phi_j = \sum_{i=1}^N a_{ij}\varphi_i \tag{19}$$

The solution presented in Eq. 19 describes a ground-state molecular orbital (MO) for systems with one electron. It therefore neglects the term for electron-electron interactions and is not descriptive enough to be applied for many-electron systems. One approach to this problem, formulated by Hartree during the early 1900s, is to form a Hamiltonian operator from a set of individual one-electron operators ($\hat{h}_i$), which satisfy the one-electron Schrödinger equation shown below.

$$\hat{h}_i \psi_i = \epsilon_i \psi_i \tag{20}$$

A product of these one-electron wave functions defines a so-called 'Hartree-product' wave function, shown in Equation 21.

$$\Psi_{HP} = \psi_1 \psi_2 \dots \psi_N \tag{21}$$

The missing electron-electron interaction term can be added to this treatment by first forming the Hartree-product wave function, and then operating on it by using the electronic Hamiltonian shown in Equation 4. Finding the correct set of orbitals, ψ, which minimize the expectation value for $\langle \Psi_{HP} | \hat{H} | \Psi_{HP} \rangle$ yields a solution in which every orbital in the set (ψ_i) is an eigenfunction of the corresponding one-electron Hamiltonian ($\hat{h}_i$), which is defined in Equation 22 below.

$$\hat{h}_i = -\frac{\hbar^2}{2m_e}\nabla_i^2 - \sum_k \frac{e^2 Z_k}{4\pi\epsilon_0 r_{ik}} + V_i\{j\} \tag{22}$$

The term $V_i\{j\}$ introduces both an approximation and a problem. The approximation stems from the fact that in this treatment electron occupying orbital i interacts with a potential from all the other electrons occupying orbitals j, and therefore the single electron on orbital i experiences an average repulsive effect.

The problem in the repulsive potential term is caused by the charge density of electrons occupying orbital j, as is presented in Equation 23 below, using atomic units.

$$V_i\{j\} = \sum_{i \neq j} \int \frac{\rho_j}{r_{ij}} \, d\mathbf{r} \tag{23}$$

Since $\rho_j = |\psi_j|^2$, the equation above refers to a wave function which it is supposed to help define. Hartree, with the help of his retired father, designed a way to find approximate solutions which circumnavigate this problem. He devised an iterative method, called the 'self-consistent field method' (or SCF method for short) in which the initial wave functions for molecular orbitals

are guessed. Inserting these guessed wave functions to Equation 21 yields a new (and possibly more accurate) set of wave functions, which are then fed in to the equations. These SCF cycles are then iterated until the change between the newly obtained functions and previous functions falls within a certain threshold, which can be picked arbitrarily. As is shown above, the SCF method allows one to compute approximate energies for molecular orbitals by operating the electronic Hamiltonian operator on the Hartree-product wave function, as shown in Equation 24 below using atomic units.

$$E = \sum_i \epsilon_i - \frac{1}{2} \sum_{i \neq j} \iint \frac{\rho_i \rho_j}{r_{ij}} \, d\mathbf{r}_i d\mathbf{r}_j \tag{24}$$

One remaining issue arises from relativistic quantum field theory, which states that a wave function describing fermions has to be antisymmetric. The Hartree product wave function presented in Equation 21 does not meet this requirement. The problem can be done away with by forming a linear combination of two-component Hartree product wave functions which are antisymmetric. An example for a 2-electron system is shown in a normalized form in Equation 25 below.

$$\Psi = \frac{1}{\sqrt{2}} \Big[\psi_a(1)\alpha(1)\psi_b(2)\beta(2) - \psi_a(2)\alpha(2)\psi_b(1)\beta(1) \Big] \tag{25}$$

The wave function presented in Equation 25 is a Slater determinantal wave function, which is often expressed in a matrix form. The general, normalized Slater determinant for a system with N electrons and χ_N spin orbitals (orbitals with both spatial and spin components) is shown below.

$$\Psi_{SD} = \frac{1}{\sqrt{N!}} \begin{bmatrix} \chi_1(1) & \chi_2(1) & \dots & \chi_N(1) \\ \chi_1(2) & \chi_2(2) & \dots & \chi_N(2) \\ \vdots & \vdots & \ddots & \vdots \\ \chi_1(N) & \chi_2(N) & \dots & \chi_N(N) \end{bmatrix} \tag{26}$$

Besides resulting in a more realistic description for a wave function, the use of a Slater determinantal wave functions leads to an important quantum phenomenon when evaluating the electrostatic repulsion between two electrons on separate orbitals with parallel spin, known as the exchange interaction. This interaction gives rise to the so-called 'Fermi hole', which is observed as a reduced probability of finding two electrons with parallel spins near each other. A brief description of the mathematics is given below.

$$\int \Psi_{SD} \frac{1}{r_{1,2}} \Psi_{SD} \; d\mathbf{r}_1 \omega_1 d\mathbf{r}_2 \omega_2 =$$
$$\frac{1}{2}\Bigg[\int |\psi_a(1)|^2 |\alpha(1)|^2 \frac{1}{r_{1,2}} |\psi_b(2)|^2 |\alpha(2)|^2 \; d\mathbf{r}_1 \omega_1 d\mathbf{r}_2 \omega_2$$
$$- 2 \int \psi_a(1)\psi_b(1) |\alpha(1)|^2 \frac{1}{r_{1,2}} \psi_a(2)\psi_b(2) |\alpha(2)|^2 \; d\mathbf{r}_1 \omega_1 d\mathbf{r}_2 \omega_2$$
$$+ \int |\psi_a(2)|^2 |\alpha(2)|^2 \frac{1}{r_{1,2}} |\psi_b(1)|^2 |\alpha(1)|^2 \; d\mathbf{r}_1 \omega_1 d\mathbf{r}_2 \omega_2 \Bigg] \tag{27}$$

The first and the last terms on the r.h.s. of Equation 27 correspond to Coulomb repulsion between two electrons, and the second term contains the so-called 'exchange integral'. Equation 27 can be further simplified by defining J_{ab} as the Coulomb integral, and K_{ab} as the exchange integral.

$$\int \Psi_{SD} \frac{1}{r_{1,2}} \Psi_{SD} \; d\mathbf{r}_1 \omega_1 d\mathbf{r}_2 \omega_2 =$$
$$\frac{1}{2}\Bigg[J_{ab} - 2 \int \psi_a(1)\psi_b(1) |\alpha(1)|^2 \frac{1}{r_{1,2}} \psi_a(2)\psi_b(2) |\alpha(2)|^2 \; d\mathbf{r}_1 \omega_1 d\mathbf{r}_2 \omega_2 + J_{ab} \Bigg]$$
$$= \frac{1}{2}\Big[J_{ab} - 2K_{ab} + J_{ab} \Big]$$
$$= J_{ab} - K_{ab} \tag{28}$$

It is noteworthy to mention that due to the orthogonality of α and β spin functions, K_{ab} vanishes when evaluated using a Slater determinantal wave function containing electrons with opposite spins.

In 1930 Vladimir Fock, a Soviet scientist, complemented Hartree's SCF method with Slater determinantal wave functions. The overall idea behind the SCF scheme remained the same, but the one-electron Hamiltonian defined in Equation 22 was replaced with a one-electron Fock operator ($\hat{f}$) which includes Coulomb integrals and exchange integrals for N orbitals, shown below in Equation 29 for a single electron i.

$$\hat{f}_i = -\frac{\hbar^2}{2m_e}\nabla_i^2 - \sum_k \frac{e^2 Z_k}{4\pi\epsilon_0 r_{ik}} + \sum_{j=1}^{N/2} (2\hat{J}_i - \hat{K}_i) \tag{29}$$

Operation on a molecular orbital wave function (χ_i) using the Fock operator yields an eigenvalue which corresponds to an orbital energy, as is shown below.

$$\hat{f}_i\chi_i = \epsilon_i\chi_i \tag{30}$$

In Equation 30 χ_i can be expanded with a set of basis functions. This treatment produces a matrix equation, which contains a Fock matrix element ($F_{\mu\nu}$) and an overlap integral ($S_{\mu\nu}$) similar to that presented in Equation 16. A secular equation defined by using these elements yields values for molecular orbital energies (E), as shown in Equation 31.

$$\begin{bmatrix} F_{11} - ES_{11} & F_{12} - ES_{12} & \dots & F_{1N} - ES_{1N} \\ F_{21} - ES_{21} & F_{22} - ES_{22} & \dots & F_{2N} - ES_{2N} \\ \vdots & \vdots & \ddots & \vdots \\ F_{N1} - ES_{N1} & F_{N2} - ES_{N2} & \dots & F_{NN} - ES_{NN} \end{bmatrix} = 0 \tag{31}$$

The Fock matrix element is defined for closed-shell systems with K basis functions in Equation 32 below.

$$F_{\mu\nu} = H_{\mu\nu}^{core} + \sum_{\lambda=1}^{K}\sum_{\sigma=1}^{K} P_{\lambda\sigma}\left[(\mu\nu|\lambda\sigma) - \frac{1}{2}(\mu\lambda|\nu\sigma)\right] \tag{32}$$

In the equation above, $H_{\mu\nu}^{core}$ is the so-called core Hamiltonian operator, and $P_{\lambda\sigma}$ are elements of the charge density matrix $\mathbf{P}$. Both are defined in Equations 33 and 34 below for M nuclei and N doubly occupied orbitals.

$$H_{\mu\nu}^{core} = \int \phi_\mu(1)\left[-\frac{1}{2}\nabla^2 - \sum_{A=1}^{M}\frac{Z_A}{|r_1 - R_A|}\right]\phi_v(1)\ d\nu_1 \tag{33}$$

$$P_{\lambda\sigma} = 2\sum_{i=1}^{N/2} c_{\lambda i}c_{\sigma i} \tag{34}$$

Using all of the definitions presented above it is possible to solve the Roothaan-Hall matrix equation, $\mathbf{FC} = \mathbf{SCE}$. The process starts with calculating the one electron integrals for the Fock matrix, $\mathbf{F}$. After these are calculated, the overlap matrix $\mathbf{S}$ is formed, diagonalised, and its inverse square root is formed ($\mathbf{S}^{-1/2}$). This is followed by guessing (or calculating) the initial charge density matrix $\mathbf{P}$, which is then used to form the two-electron integrals and to complete the Fock matrix. A new matrix $\mathbf{F}' = \mathbf{S}^{-1/2}\mathbf{F}\mathbf{S}^{-1/2}$ is then formed, which can then be utilized in a secular equation $|\mathbf{F}' - \mathbf{EI}|$. The secular equation yields eigenvalues $\mathbf{E}$ and eigenvectors $\mathbf{C}'$. Molecular orbital

coefficients $\mathbf{C} = \mathbf{S}^{-1/2}\mathbf{C}'$ are then calculated. The cycle ends by forming a new charge density matrix, and by checking whether or not the system has converged. If not, a new Fock matrix is formed using the new charge density matrix, and the cycle is then repeated until convergence criteria are met.

All of this results in a set of molecular orbitals with corresponding values for energy, ϵ. The orbital energy is defined as a sum of the core interaction (from H^{core}), the Coulomb interaction, and the exchange interaction, as is shown below.

$$\epsilon_i = H_i^{core} + \sum_{j=1}^{N/2}(2J_{ij} - K_{ij}) \tag{35}$$

The total energy can then be defined as follows.

$$E = \sum_{i=1}^{N}\epsilon_i - \sum_{i=1}^{N/2}\sum_{j=1}^{N/2}(2J_{ij} - K_{ij}) \tag{36}$$

The subtraction in Equation 36 is carried out in order to avoid double counting, as J_{ij} and K_{ij} are already included when calculating ϵ_i.

The treatment above has been limited to closed-shell singlet systems (RHF), where each molecular orbital is either doubly occupied or empty. It should be noted that the HF method can be extended to include open-shell systems via the spin-restricted Hartree-Fock theory (ROHF), or the spin-unrestricted Hartree-Fock theory (UHF). The UHF treatment contains separate sets of molecular orbitals for α spin electrons and β spin electrons, with two corresponding charge density matrices. The ROHF method is not as flexible, as it still has the same spatial functions for electrons of both spins (α and β).

A final note should be made about the general limit of the Hartree-Fock method. Due to the use of a single Slater determinant, some electron correlation effects are not captured in this method. If a full basis set could be utilized, the method could reach the so-called Hartree-Fock limit, which lies above the true ground-state. The difference in energy between the HF limit and the true (non-relativistic) ground-state is known as correlation energy, named after Coulomb correlation which is missing from HF methods. Some of the correlation can be captured by implementing perturbed models (MP2 etc.) or by introducing multiple determinants.

2.3 Density Functional Theory

The main concept in DFT is to circumnavigate the tedious tasks and problems associated with extracting physicochemical information from a wave function. This is achieved by relating the electronic energy of the studied system to the electron density of the said system. In more concise terms, DFT starts with the assumption that the electronic energy of the system is a functional of the electron density. The related mathematical notation is given in equation 37 below.

$$E[\rho(\mathbf{r})] = \int V_{ext}(\mathbf{r})\rho(\mathbf{r})\ d\mathbf{r} + F[\rho(\mathbf{r})] \tag{37}$$

In Equation 37 above, the external potential, $V_{ext}(\mathbf{r})$, arises from the electron-nuclei Coulomb interaction and the term $F[\rho(\mathbf{r})]$ contains a sum of the kinetic energy of the electrons, as well as the energy contribution from electron-electron interactions.

The first steps towards implementing methods based on electron density were taken in the 1920s, when Fermi and Thomas published their work on uniform electron gasses. This was followed by the work of Slater in the 1950s, which, unlike the very inaccurate Thomas-Fermi method, was accurate enough to be implemented in solid-state physics.

In the 1960s Walter Kohn and Pierre Hohenberg published two critical proofs: The 'Hohenberg-Kohn existence theorem' and the 'Hohenberg-Kohn variational theorem'. The existence theorem states that the ground-state electron density is enough to define the Hamiltonian operator for a given system, and thus yields a value for the ground-state energy (among other physical properties). Using a proof by contradiction, they showed that only a single external potential, $V_{ext}(\mathbf{r})$, corresponds to a single nondegenerate state of the system (such as the ground-state).

The proof starts by assuming that there are two separate potentials (V_i and V_j) which both determine the same ground-state density, ρ_0. Both potentials have their associated Hamiltonian operators ($\hat{H}_i$ and $\hat{H}_j$), and both Hamiltonian operators have their corresponding ground-state wave functions ($\Psi_{0,i}$) and associated eigenvalues ($E_{0,i}$). By applying the variational theorem described in the previous section, it is possible to show that operating $\hat{H}_i$ on the wave function Ψ_j results in an expectation value which is larger than $E_{0,i}$, shown more precisely in Equation 38 below.

$$E_{0,i} < \langle \Psi_{0,j} | \, \hat{H}_i \, | \Psi_{0,j} \rangle \tag{38}$$

Equation 38 can be rewritten as follows.

$$\begin{aligned} E_{0,i} &< \langle \Psi_{0,j} | \, \hat{H}_i - \hat{H}_j + \hat{H}_j \, | \Psi_{0,j} \rangle \\ &< \langle \Psi_{0,j} | \, \hat{H}_i - \hat{H}_j \, | \Psi_{0,j} \rangle + \langle \Psi_{0,j} | \, \hat{H}_j \, | \Psi_{0,j} \rangle \\ &< \langle \Psi_{0,j} | \, V_i - V_j \, | \Psi_{0,j} \rangle + E_{0,j} \end{aligned} \tag{39}$$

If potentials $V_{i,j}$ are one-electron operators, the final inequality can be re-written in a form which includes the ground-state density.

$$E_{0,i} < \int \Big[V_i(\mathbf{r}) - V_j(\mathbf{r}) \Big] \rho_0(\mathbf{r}) \; d\mathbf{r} + E_{0,j} \tag{40}$$

Since i and j can be freely interchanged, Equation 40 can be rewritten in the following way.

$$E_{0,j} < \int \Big[V_j(\mathbf{r}) - V_i(\mathbf{r}) \Big] \rho_0(\mathbf{r}) \; d\mathbf{r} + E_{0,i} \tag{41}$$

With the assumption that the ground-state densities are the same for both i and j, the addition of Equations 40 and 41 results in the following contradiction.

$$\begin{aligned} E_{0,i}+E_{0,j} &< \int \Big[V_j(\mathbf{r}) - V_i(\mathbf{r}) \Big] \rho_0(\mathbf{r}) \; d\mathbf{r} + \int \Big[V_i(\mathbf{r}) - V_j(\mathbf{r}) \Big] \rho_0(\mathbf{r}) \; d\mathbf{r} + E_{0,i} + E_{0,j} \\ &< \int \Big[V_j(\mathbf{r}) - V_i(\mathbf{r}) + V_i(\mathbf{r}) - V_j(\mathbf{r}) \Big] \rho_0(\mathbf{r}) \; d\mathbf{r} + E_{0,i} + E_{0,j} \\ &< E_{0,i} + E_{0,j} \end{aligned} \tag{42}$$

The contradiction presented in Equation 42 proves that the external potential is defined by the non-degenerate ground-state density. Moreover, knowing the density allows the determination of the Hamiltonian operator, which in turn allows the determination of the wave function. Although the proof presented above, coupled with the Hohenberg-Kohn variational theorem, has interesting and important consequences, it only yields solutions when the respective Hamiltonian operator is employed (just like in the HF method), which is not in line with the DFT 'philosophy' of not having to deal with

the Schrödinger equation. In other words, the Hohenberg-Kohn equations do not enjoy from any speedup when compared to the HF method.

All of this changed in 1965 when Kohn and Sham published the framework for the Kohn-Sham self-consistent field method. Their reasoning started with the notion that a system consisting of nuclei and *noninteracting* electrons can be described with a Hamiltonian operator which consists of a sum of one-electron operators. The system with noninteracting electrons can then be chosen so that the electron density is identical to an electron density of some real system where electrons interact normally. Since electron density defines the system (e.g. location of nuclei and their atomic numbers), the difference between the fictitious and real system must be due to the electron-electron and electron-nuclei interactions. The energy functional of such a system can be expressed with the following terms.

$$E[\rho(\mathbf{r})] = T_e[\rho(\mathbf{r})] + V_{n-e}[\rho(\mathbf{r})] + V_{e-e}[\rho(\mathbf{r})] + \Delta T[\rho(\mathbf{r})] + \Delta V_{e-e}[\rho(\mathbf{r})] \quad (43)$$

The first three terms on the r.h.s of Equation 43 describe the kinetic energy of electrons in a noninteracting system, electron-nuclei interaction, and Coulomb repulsion between the electrons. $\Delta T[\rho(\mathbf{r})]$ and $\Delta V_{e-e}[\rho(\mathbf{r})]$ are so-called correction terms, which describe the correction to the kinetic energy of the nuclei due to electron interactions, and the correction to the electron-electron interactions, which has to be taken into account since the $V_{e-e}[\rho(\mathbf{r})]$ term omits all non-classical effects. Equation 43 can be rewritten using an orbital expression for density, as is shown below.

$$\begin{aligned} E[\rho(\mathbf{r})] = &\sum_i^N \left(\left\langle \chi_i \right| -\frac{1}{2}\nabla_i^2 \left| \chi_i \right\rangle - \left\langle \chi_i \right| \sum_k^M \frac{Z_k}{|\mathbf{r}_i - \mathbf{r}_k|} \left| \chi_i \right\rangle \right) \\ &+ \sum_i^N \left\langle \chi_i \right| \frac{1}{2} \int \frac{\rho(\mathbf{r}')}{|\mathbf{r}_i - \mathbf{r}'|} \, d\mathbf{r}' \left| \chi_i \right\rangle + E_{xc}[\rho(\mathbf{r})] \end{aligned} \quad (44)$$

Equation 44 represents a system with N electrons and M nuclei (i runs over electrons, k over nuclei). E_{xc} contains both correction terms from Equation 43, and is often referred to as the exchange-correlation term (thus the subscript 'xc'). Density of the Slater determinantal wave functions is given by the following equation.

$$\rho = \sum_i^N |\chi_i|^2 \quad (45)$$

Selecting orbitals in a way which minimizes the value of energy in Equation 44 can be shown to obey the following equation.

$$\hat{h}^{KS}\chi_i = \epsilon_i\chi_i \tag{46}$$

In Equation 45 $\hat{h}^{KS}$ is the Kohn-Sham one-electron operator, which is defined as follows.

$$\hat{h}^{KS} = -\frac{1}{2}\nabla^2 - \sum_k^M \frac{Z_k}{|\mathbf{r}-\mathbf{r}_k|} + \int \frac{\rho(\mathbf{r}')}{|\mathbf{r}-\mathbf{r}'|}\, d\mathbf{r}' + V_{xc} \tag{47}$$

In Equation 47, the last term is defined as a functional derivative $V_{xc} = \dfrac{\delta E_{xc}}{\delta\rho}$.

As in the HF method, the following task is to form a secular determinant from a selected basis set (ϕ). The Fock matrix elements can now be substituted with the Kohn-Sham matrix elements $K_{\mu\nu}$.

$$K_{\mu\nu} = \langle\phi_\mu|\, \hat{h}^{KS}\, |\phi_v\rangle \tag{48}$$

Due to the presence of electron density in the equations, an iterative SCF method must be employed.

Although the mathematical treatment is rather similar in both the HF method and in the DFT method, a fundamental difference can be found between the two. DFT starts from an exact statement and yields approximate results due to the unknown exchange-correlation term which has to be approximated, whereas the Hartree-Fock method is non-exact to begin with.

A final note should be made about the variational properties of the DFT method. Whilst the exact formulation of the method is variational (meaning that any state of the system obtained is equal to, or higher in energy than the ground-state of the system), the approximations for the exchange-correlation term are not. This can be proven by comparing the DFT energies for a single hydrogen atom (for which the Schrödinger equation can be solved exactly) to the actual values of energy. Depending on the functional used to approximate V_{xc}, the energies can be lower than the ground-state energy.

3 Background and Methods

The work described in this thesis focused on two types of Zintl ion systems, originally published by Dr. J. M. Goicoechea and Prof. S. C. Sevov in 2005. [19, 20]

The first publication focused mainly on germanium clusters of the type $[Ni@(Ge_9Ni - L)]^{n-}$. In the three cases relevant to the work presented in this document, the ligand L was either CO, C_2Ph, or PPh_3, and the charge state was either $n = 2$ or $n = 3$. These structures are presented in Figure 3 below.

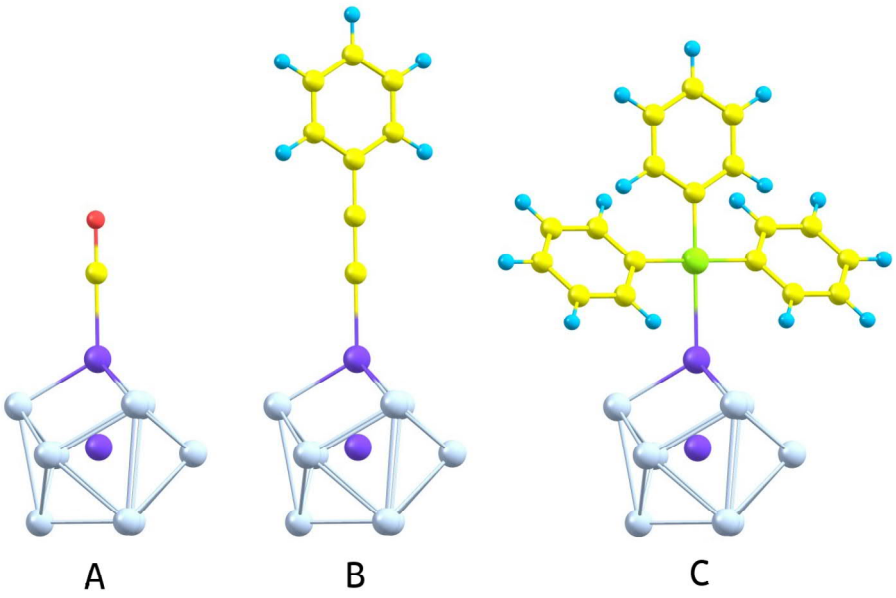

Figure 3: Structures from Ref. 19. A = $[Ni@(Ge_9Ni - CO)]^{2-}$, B = $[Ni@(Ge_9Ni - C_2Ph)]^{3-}$, and C = $[Ni@(Ge_9Ni - PPh_3)]^{2-}$. Atoms are coloured in the following way: grayish blue for germanium, yellow for carbon, red for oxygen, purple for nickel, and turquoise for hydrogen. This colouring scheme will be used throughout the rest of this document. Image drawn with Chemcraft.

The second paper described a system consisting of two Ge_9 clusters, analogous to the germanium compounds in Ref. 19. The dimeric system has a linear triatomic nickel filament, which connects the Ge_9 clusters through the centermost nickel. The system ($[(Ni - Ni - Ni)@(Ge_9)_2]^{4-}$) is presented in Figure 4.

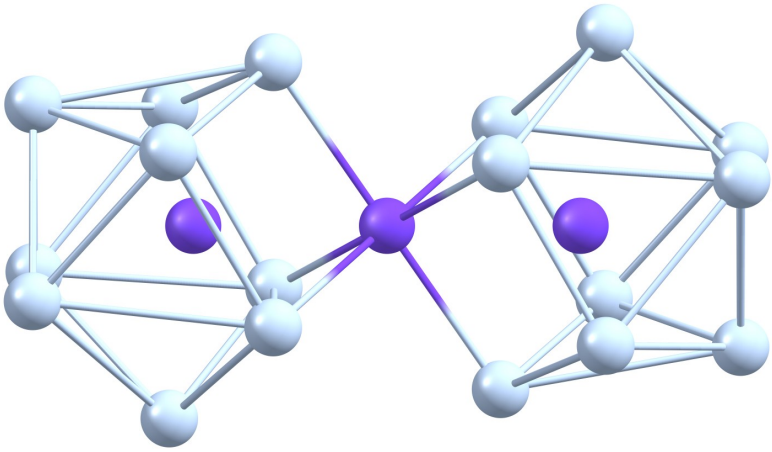

Figure 4: Structure from Ref. 20, $[(Ni-Ni-Ni)@(Ge_9)_2]^{4-}$. Colour scheme is the same as in Figure 3. Image drawn with Chemcraft.

Although the focus in the original publications was mainly on the synthesis and characterization of these compounds, the authors made some interesting claims about the electronic structure of the systems, which were thought to be worth investigating further. The first peculiarity arose from the claim that the systems described in Ref. 19 and in Figure 3 should be considered to be electron-deficient *closo* species with 20 cluster-bonding electrons. This seemed to be in contradiction with the fact that the clusters have an opened face, associated with a *nido* species, which contains 22 cluster-bonding electrons. The opened face is highlighted in Figure 5 below.

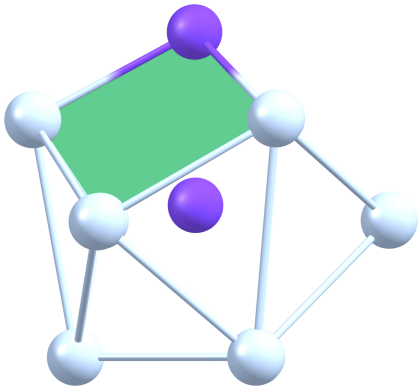

Figure 5: $[Ni@(Ge_9Ni)]^{2-}$, with one of the opened faces highlighted in green. Colour scheme is the same as in Figure 3. Image drawn with Chemcraft.

The second point of interest was the claim that the outer nickel and the ligand (henceforth named as 'capping fragment') do not donate any electrons to the cluster. Finally, the authors had extended the same logic from their previous

work on single clusters to the dimeric system in Ref. 20 (illustrated in Figure 4), asserting that the three nickels in the filament have a $3d^{10}$ electron configuration, and thus will not make any contributions to the cluster-bonding electron count.

The aim of the work presented in this thesis was to utilize DFT and CAS-SCF methods to explore the validity of the aforementioned claims, and to see if any further information about the electronic structure of these clusters could be revealed through the use of computational methods.

3.1 Single clusters

Initial starting configurations for the three compounds presented in Figure 3 were obtained from Ref. 19 and were built using the Chemcraft software package.[2] The phenyl groups in compounds B and C (see Fig. 3) were replaced with hydrogens, as they were deemed to be unnecessary for assessing the electronic structure of the cluster and the electrostatic interactions between the cluster and the ligand. The 'simplified' versions of these compounds are presented in Figure 6 below.

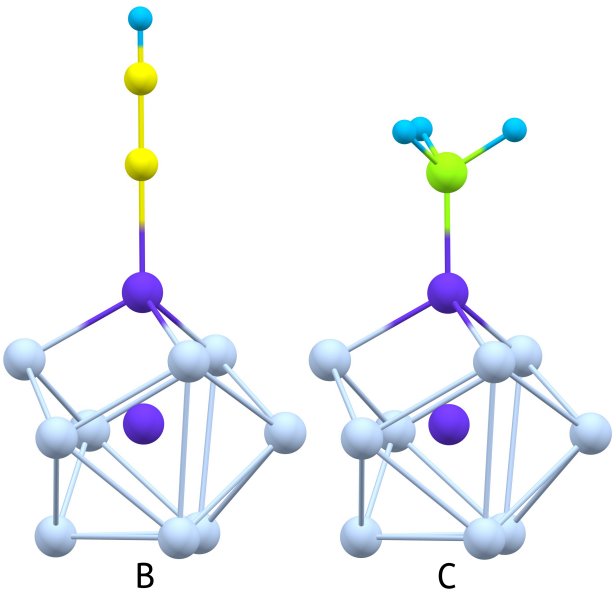

Figure 6: Modified compounds from Ref. 19. See Figure 3 for the original structures. The ligand PPh_3 is now PH_3 and the ligand C_2Ph is now C_2H. Colour scheme is the same as in Figure 3. Image drawn with Chemcraft.

[2]No proper citation given. Visit the Chemcraft webpage for more information.

The three original structures were initially complemented with analogous compounds containing the following ligands: CN, NO, and PF_3. A structure with no ligand attached, $[Ni@(Ge_9Ni)]$, was also included in to the calculations. A total of 14 systems were initially created. Half of the systems were in the point group C_{3v}, corresponding to a 20 cluster-bonding electron *closo*-system, and the other half were in the point group C_{4v}, corresponding to a 22 cluster-bonding electron *nido*-system. Figure 7 below shows the $[Ni@(Ge_9Ni)]$ cluster in both C_{3v} and C_{4v} symmetries.

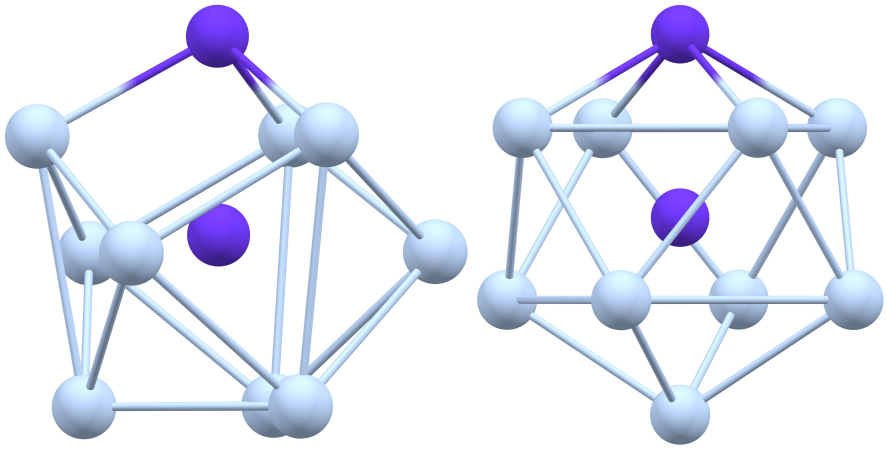

Figure 7: The bare cluster in C_{3v} (left) and C_{4v} (right) symmetry. Colour scheme is the same as in Figure 3. Image drawn with Chemcraft.

Gas phase geometry optimization, frequency and population analysis were performed to both sets of systems with the Gaussian09 software package [21], using B3LYP and BLYP functionals. [22, 23, 24] Both functionals were used in junction with the SDD basis set[3]. For each system, the values for total energy, LUMO-HOMO gap, and intermolecular distances (such as the distance between the interstitial and capping nickel atom) were recorded. In addition, the number of imaginary frequencies was monitored to verify whether the geometry optimization routines had converged to a true minimum. Two of the systems, with ligands PH_3 and PF_3, produced problems due to the symmetry present in the ligand. These systems were discarded, and no further calculations were performed on these systems.

The same calculations were repeated with a polarizable continuum model (PCM), which was implemented in order to capture any solvent effects. The electrostatic interaction between the germanium cluster and the ligand

[3] See the Gaussian webpage for a list of references.

was assessed using two strategies. The first approach was to examine the change in total energy difference between C_{3v} and C_{4v} systems when moving from electron donating ligands (CN^-) towards electron withdrawing ligands (NO^+). The second method used introduced new ligands H^-, Cl^-, and F^-. These ligands were used to reveal information about the behaviour of the cluster's frontier orbitals, since H^- interacts only via σ bonding, whereas Cl^- and F^- interact also through π-interactions.

All of the aforementioned calculations were repeated for two other sets of systems, where one of the nickel atoms had been changed to a cobalt atom (either the interstitial or capping nickel). The methods used in these calculations were the same as those described above. Due to their limited relevance to this thesis, the results and exact methods used for the $[Ni@(Ge_9Co-L)]^{n-}$ and $[Co@(Ge_9Ni-L)]^{n-}$ systems are omitted.

3.2 Dimer

The starting structure was obtained from Ref. 20 and the initial configuration was built using Chemcraft. Keeping in line with the work performed on single clusters, a model was built for both C_{3v} and C_{4v} symmetries. A geometry optimization, population and frequency analysis was performed for both systems using the same functionals and basis set as with the single clusters.

Further analysis on the electronic structure was performed using the MOLCAS software package. [25] The analysis began with a standard HF level calculation with a full population analysis. Solvent effects were taken into account by implementing a PCM solvent model. The resulting molecular orbitals were then visualized and analyzed using the MOLCAS grid and geometry viewer software (henceforth abbreviated as GV). Relevant orbitals were visualized and selected using the GV software, and used in a Restricted Active Space (henceforth abbreviated as RAS) SCF calculation. These calculations used the ANO-RCC-MB basis set and a PCM solvent model. Although the system was prepared in C_{3v} symmetry, C_{2h} point group was utilized due to limitations in the MOLCAS software. [4]

The RAS-SCF calculations began with a [2,2] configuration (2 active electrons, 2 active orbitals). Both of the selected molecular orbitals had a strong

[4]MOLCAS is able to use higher symmetries, but this requires non-standard user input.

d_{z^2} component. The active space (number of active electrons and orbitals) was then gradually expanded, until all the relevant molecular orbitals could be included with a sufficient electron population. In the case of $[(Ni-Ni-Ni)@(Ge_9)_2]^{4-}$ the sufficient configuration included 8 active electrons and seven active orbitals. Four of the active orbitals were picked from the first symmetry species (A_g), two from the second group (B_g), and the final active orbital was placed in the fourth symmetry species (B_u). The overall setup for the [8,7] RAS-SCF calculation is given in Table 1 below.

Table 1: The basic parameters for a [8,7] RAS-SCF calculation.

Symmetry Species	A_g	B_g	A_u	B_u
Active (RAS2) Orbitals	4	2	0	1
Inactive Orbitals	98	66	67	97
Secondary Orbitals	11	8	10	14
Basis Functions	113	76	77	112

Some of the molecular orbitals from the HF calculations are presented in Figure 8 below.

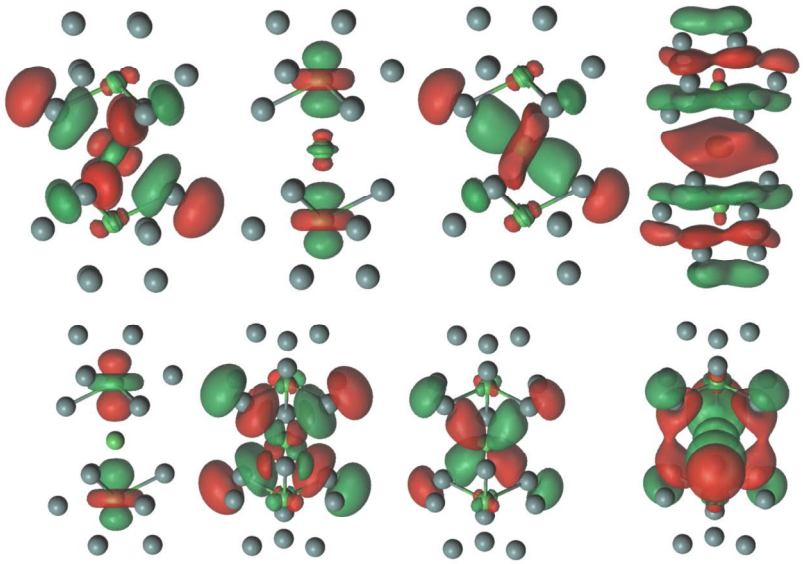

Figure 8: Orbitals obtained from the HF calculation. Seven of these orbitals were included in the RASSCF calculation. Both ends of the nickel filament have three bonds visible, and the rest of the *Ge* cluster is drawn without bonds. Image produced with the GV software.

4 Results

Several different data points were initially gathered from each calculated system. These included the total system energy, size of the LUMO-HOMO gap, $Ni - Ni$ distance, capping $Ni-$ligand distance, distances from the interstitial Ni to the Ge atoms, horizontal $Ge - Ge$ distances, and vertical $Ge - Ge$ distances. The number of imaginary frequencies and strength of certain frequencies (such as the $\sim$1860 cm^{-1} $C = O$ vibration) were measured. In the final phase of the analysis, molecular orbitals of each system were analyzed. This was performed first through visual inspection, and after the relevant orbitals had been identified the inspection continued with more emphasis on the numerical values. In practice this meant extracting the relevant eigenvalues of the molecular orbitals from the Gaussian09 output files.

During the analysis it became evident that the focus should be placed towards the energies of the studied systems, and some of the initial 'structural observables' (such as certain intermolecular distances) were discarded from further analysis due to their limited relevance to the questions at hand. The initial results obtained from calculations performed in vacuum were also discarded from the final analysis. This was due to the anionic state of the systems, which required a solvent model in order to capture all the polarization effects.

The DFT calculations for $[(Ni - Ni - Ni)@(Ge_9)_2]^{4-}$ were used mainly for obtaining information about the molecular orbitals, which in turn was used to select the correct orbitals for the RAS-SCF calculation. The analysis performed on these calculations was relatively superficial, and thus the focus of this work will be on the results obtained from the RAS-SCF calculations.

4.1 Single Clusters

Three of the different observed parameters are presented here for both C_{3v} and C_{4v} systems, and for both functionals used (B3LYP and BLYP). These are the size of the LUMO-HOMO gap, Ni-Ni distance, and the difference in total energy between the C_{3v} and C_{4v} systems with same ligands.

Two trends were observed when analyzing the LUMO-HOMO gap. The first and most obvious observation was that B3LYP predicts $\sim$1.3 eV higher values for the LUMO-HOMO gap, regardless of the symmetry. The second trend can be observed in the systems with C_{3v} symmetry when moving from the electron donating ligand (CN^-) to the electron withdrawing ligand (NO^+). It seems

that the C_{3v} systems become less stable if the capping fragment contains an electron withdrawing ligand. The weakened stability can in this case be observed as a decrease in the size of the LUMO-HOMO gap. Interestingly, the same effect is not observed in the C_{4v} systems, in which these effects seem to be less pronounced. The data for both systems and both functionals is illustrated in figure 9 below.

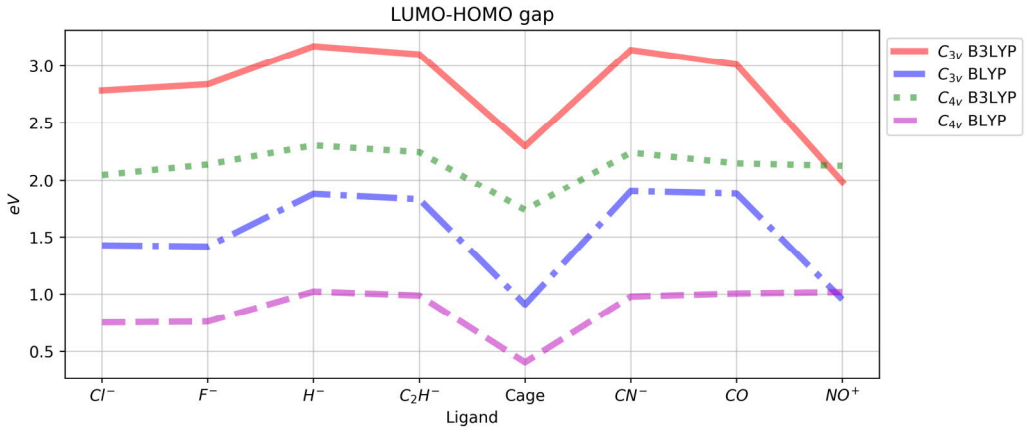

Figure 9: The LUMO-HOMO gap for both symmetries and both functionals. 'Cage' refers to a system where the capping Ni is in place, but has no ligand attached to it.

The distance between the interstitial Ni atom and the capping Ni atom underwent relatively unremarkable changes when the ligands were varied, with the largest deviation being approximately 0.10 Å. The only outliers were observed in the case of NO^+ ligand, where the systems with C_{4v} symmetry had a longer $Ni - Ni$ distance than their C_{3v} point group counterparts. Further analysis on the $[Ni@(Ge_9Ni - NO)]^{1-}$ revealed that the ligand was non-linear in C_{3v} systems, deviating approximately 10° from the linear angle. C_{4v} systems were observed to have a $Ni - N - O$ angle of 180°. The C_{3v} systems had a vibrational frequency of 1680 cm^{-1}, whereas the C_{4v} systems had the same vibration at 1660 cm^{-1}.

Based on these observations, it can be argued that the electron withdrawing effect of the NO^+ ligand is more pronounced in the C_{3v} systems, decreasing the electron density on the cluster and shifting it to the $N - O$ bond. The data for $Ni - Ni$ distances is shown below in Figure 10.

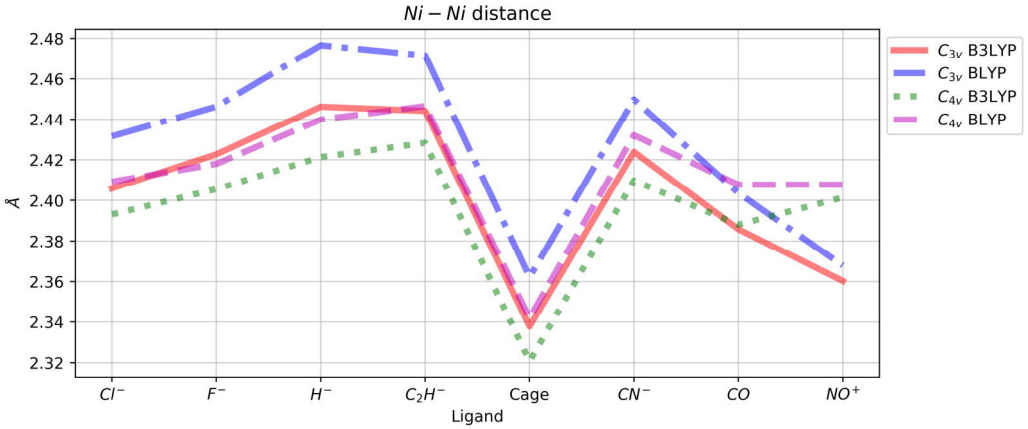

Figure 10: The $Ni - Ni$ distance in ångströms for all systems.

Both the linear and bent system are drawn in Figure 11 below.

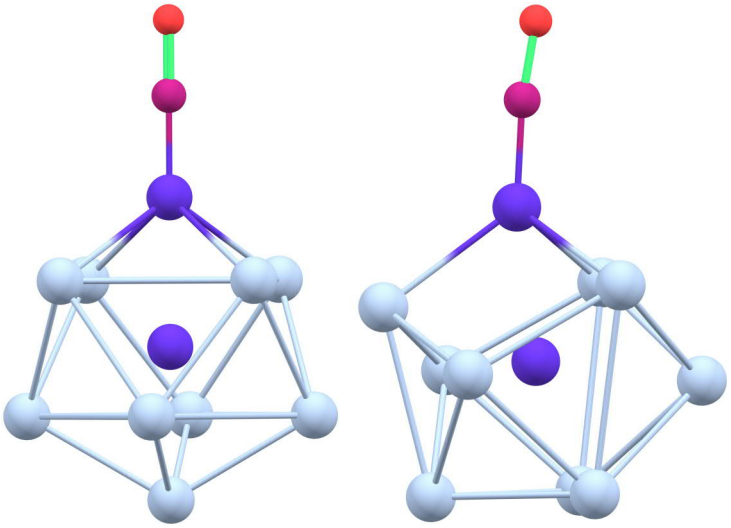

Figure 11: The C_{4v} system with a linear NO ligand (on the left), and the C_{3v} system with the bent ligand (on the right). Colour scheme is the same as in Figure 3. Image drawn with Chemcraft.

The final parameter described here is the difference in total energy between the C_{3v} and the C_{4v} systems. The difference was calculated simply by subtracting the total energy of the C_{4v} system from the corresponding value for a C_{3v} system. The relevant data is presented in Figure 12 below for both functionals.

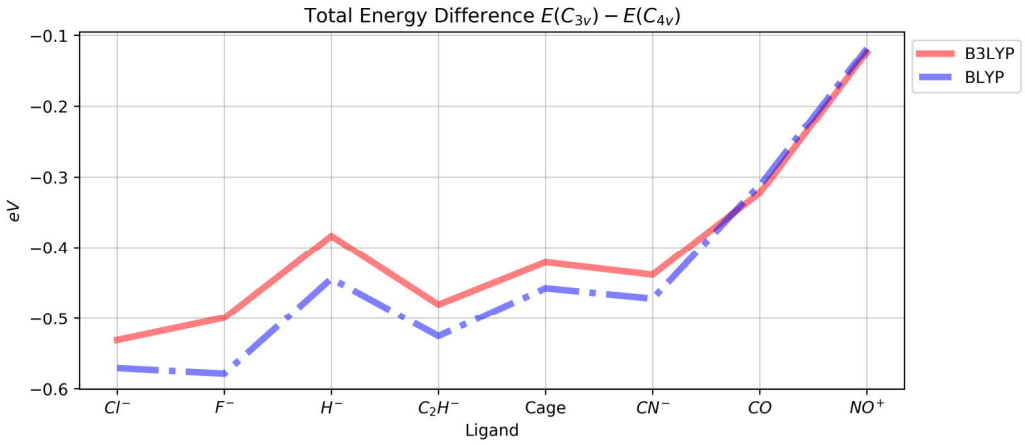

Figure 12: The total energy difference between the C_{4v} and C_{3v} systems.

Figure 12 shows two trends: One can be observed when moving from Cl^- to H^-, and the other when moving from CN^- to NO^+. The latter trend is showing how the C_{4v} symmetry becomes more stable as the electron donating ligand is replaced with electron withdrawing ligand. For the three last ligands (CN^-, CO, and NO^+) there is only a ~ 0.02 eV difference between the energies predicted by the two different functionals, indicating that the increased stability of the C_{4v} system predicted by the calculations is not dependent on the functional.

The former trend shows an increased stability for C_{4v} systems when the ligand is changed from a π-donor, Cl^-, to a σ-donor, H^-. This initially contradictory observation was explained by the position of the frontier molecular orbitals. In C_{4v} symmetry, the frontier molecular orbitals are placed on top of the cluster, enabling more effective interaction with the ligand. In C_{3v} symmetry the frontier molecular orbitals are mainly located on the sides of the Ge_9 cluster, away from the ligand. This placement is illustrated in Figures 13 and 14 below, which show the highest occupied molecular orbital for $[Ni@(Ge_9Ni)]^{2-}$ with both C_{3v} and C_{4v} symmetry.

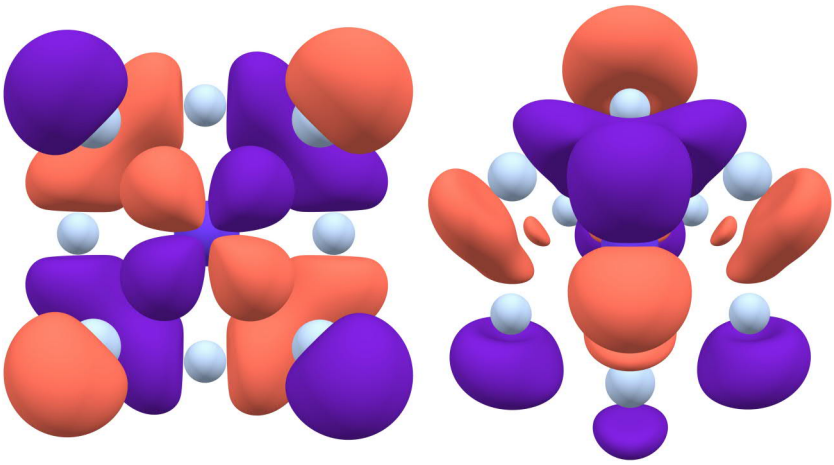

Figure 13: Highest occupied molecular orbitals for C_{4v} (left) and C_{3v} (right) systems. In this image the 'camera' is looking down the z-axis. No bonds are drawn in order to clarify the image. Colour scheme is the same as in Figure 3. Image drawn with Chemcraft.

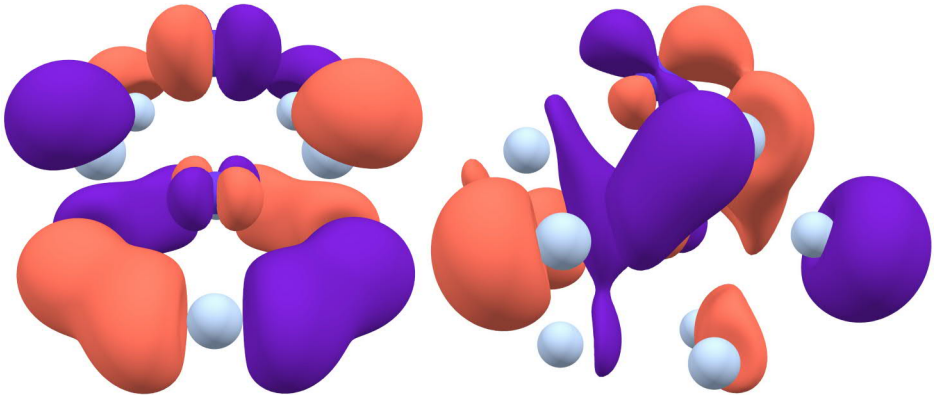

Figure 14: Highest occupied molecular orbitals for C_{4v} (left) and C_{3v} (right) systems. In this image the 'camera' is looking down the y-axis. No bonds are drawn in order to clarify the image. Colour scheme is the same as in Figure 3. Image drawn with Chemcraft.

4.2 Dimer

The final analysis presented in this work focuses on the occupation numbers of the molecular orbitals present in the $[(Ni-Ni-Ni)@(Ge_9)_2]^{4-}$ system. These were obtained through restricted active space SCF calculations, as described in the 'Methods' section. As mentioned in the previous section, the size of the active space was increased until all the relevant orbitals had been included, which in practice meant a [8,7] configuration. Once the system had successfully converged, CI-coefficients and natural orbital occupation

numbers were obtained from the output, along with grid-files containing 3-dimensional representations of the relevant molecular orbitals.

The CI-coefficients yield information about the multi-configurational nature of the studied system (or the absence of it), with integer values for orbital occupancies (doubly occupied, singly occupied, and empty) and corresponding weights. These are listed in table 2 below for the studied $[(Ni-Ni-Ni)@(Ge_9)_2]^{4-}$ system.

Table 2: CI-coefficients from the [8,7] active space. Occupancies are given for symmetry species 1, 2, and 4 since no orbitals were included from the A_u symmetry species. '2' refers to a fully occupied molecular orbital, 'u' and 'd' refer to a singly occupied orbital with spin up or down, and '0' refers to an empty orbital.

	Symmetry species			
1111	**22**	**4**	**Coefficient**	**Weight**
2220	20	0	0.60136	0.36164
2220	02	0	-0.14074	0.01981
u22d	ud	0	-0.15952	0.02545
u22u	dd	0	0.05363	0.00288
2200	20	2	-0.67920	0.46132
2200	02	2	0.15692	0.02462
0222	20	0	-0.14080	0.01982
u20d	ud	2	-0.17819	0.03175
u20u	dd	2	0.05963	0.00356
u20d	02	2	0.05444	0.00296
0202	20	2	0.15699	0.02464
0202	ud	2	-0.05448	0.00297

In a simplistic way of thinking, the final state of the active space can be thought as a combination of the configurations listed in Table 2 above. The weights indicate that there are two major contributors: *2220 20 0* and *2200 20 2*. The fact that two states have significant weights indicates that the $[(Ni-Ni-Ni)@(Ge_9)_2]^{4-}$ system truly has a multi-configurational nature.

Based on the data presented above, MOLCAS is able to calculate natural orbital occupation numbers for the molecular orbitals included in the active space. These occupation numbers are presented in Table 3 below.

Table 3: The natural orbital occupation numbers for all the seven active orbitals.

Symmetry species	**1**	**2**	**3**	**4**
A_g	1.821298	1.996901	0.881727	0.179203
B_g	1.821385	0.179118	-	-
B_u	1.120368	-	-	-

Table 3 shows one fully occupied orbital at $A_g(2)$. Three pairs can be observed: $B_u(1)$ - $A_g(3)$, $B_g(1)$ - $B_g(2)$, and $A_g(1)$ - $A_g(4)$. These are illustrated in Figures 15 through 18 below.

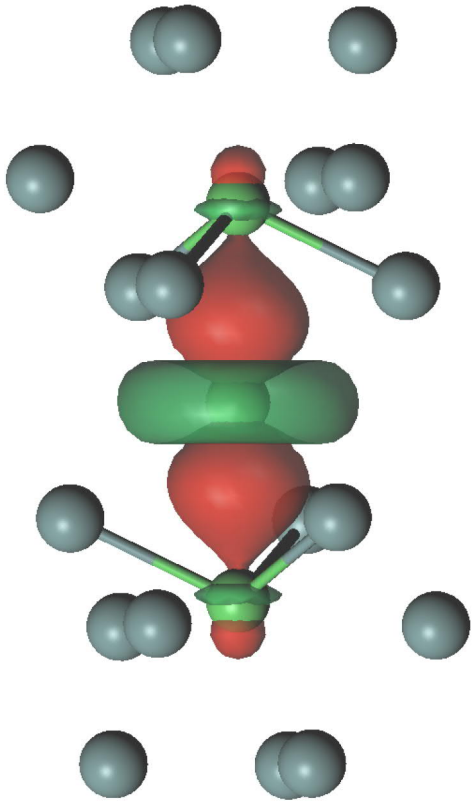

Figure 15: The fully occupied molecular orbital from the A_g symmetry species. The orbital has only d_{z^2} and $d_{x^2-y^2}$ character, and describes bonding between central Ni and the rest of the filament. Figure drawn with the GV software.

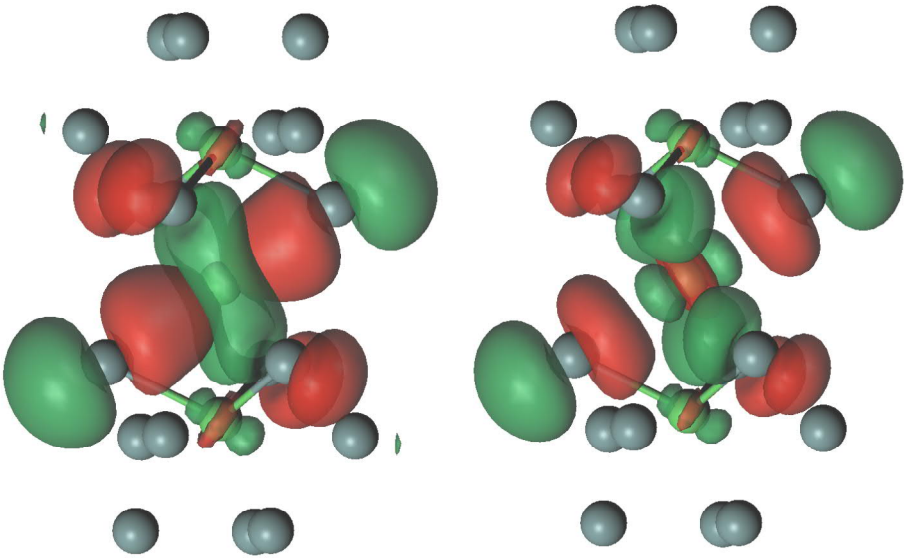

Figure 16: Orbital pair $A_g(1)$ - $A_g(4)$. The $A_g(1)$ molecular orbital on the left describes $Ni - Ge$ bonding through the ends of the $Ni - Ni - Ni$ filament. The $A_g(4)$ molecular orbital on the right is the corresponding antibonding orbital. Figure drawn with the GV software.

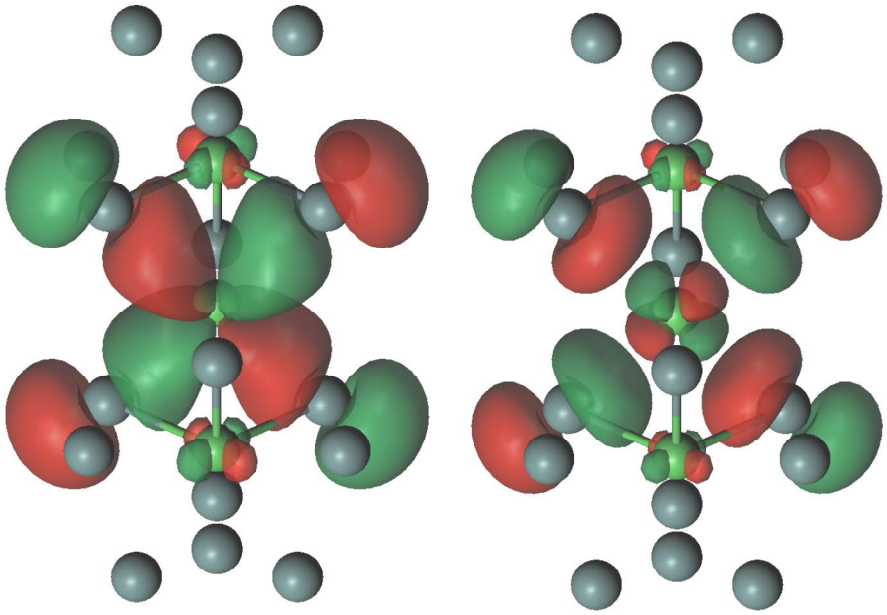

Figure 17: Orbital pair $B_g(1)$ - $B_g(2)$. Figure drawn with the GV software.

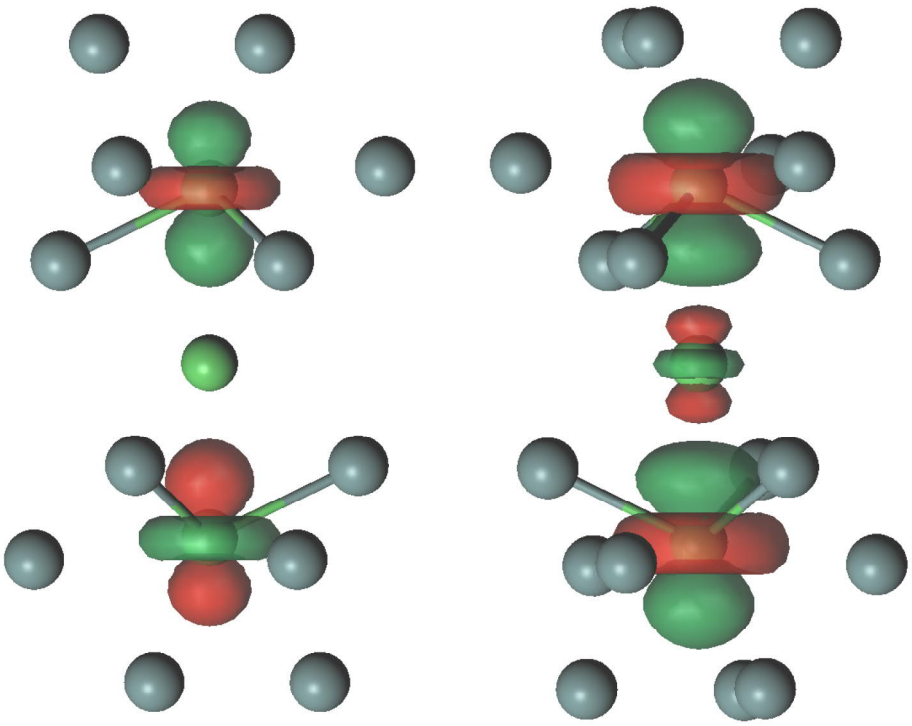

Figure 18: Orbital pair $B_u(1)$ - $A_g(3)$. Figure drawn with the GV software.

5 Conclusions

Based on the calculations performed, several conclusions are available. Firstly, the DFT calculations performed on the so-called single clusters quite definitely show that the nature of the ligand attached to the $[Ni@(Ge_9Ni-L)]^{n-}$ system has clear effects on the rest of the compound. This was observed as changes in the LUMO-HOMO gap, intermolecular distances and total energies. Further examination of the frontier orbitals revealed that symmetry has a significant effect on the cluster-ligand interactions. In C_{3v} symmetric systems the frontier orbitals are residing mainly on the sides of the cluster, thus resulting in weaker interactions with the ligand, whereas in the C_{4v} symmetric systems the frontier orbitals mainly reside on top of the cluster, enabling stronger π-interactions between the ligand and the cluster.

The DFT calculations also cast some doubt on the total charge of -2 asserted by Ref. 19. The data presented in Section 3 (especially in Figure 12) suggests that the electron counting rules employed were not able to take into account all the relevant interactions present in the $[Ni@(Ge_9Ni-L)]^{n-}$ systems. The work presented here has shown that there in fact is electrostatic interactions between the capping fragment and the rest of the compound. Definite quantification of these interactions is likely to require more work with more sophisticated computational tools, as well as more collaboration between theoretical and applied chemistry.

The RASSCF calculations seem to suggest that the Ni filament of the $[(Ni-Ni-Ni)@(Ge_9)_2]^{4-}$ system is not as inactive as claimed by Ref. 20. The data, presented in Tables 2 and 3, suggests that the caps of the triatomic filament reside in $3d^9$ configuration, instead of the claimed $3d^{10}$ configuration. This in turn implies that the whole system has an overall charge of -6, instead of the suggested -4. The fact that the compound characterized in Ref. 20 is EPR silent suggests that the proposed $[(Ni-Ni-Ni)@(Ge_9)_2]^{6-}$ system resides in a singlet diradical state.

Acknowledgments

I owe my sincerest gratitude to Professor John McGrady, who took me in to his group, introduced me to the topic of this thesis, and supervised this work. I would also like to acknowledge the great help received from Dr. Xiao Jin.

My deepest thanks go to Professor Jukka Lukkari. His supervision and help with this thesis is greatly appreciated, as is the general support he has given throughout my studies.

Thanks to Dr. Henri Kivelä for supervising this thesis. I would also like to thank him for the countless times he has taken time to answer one of my seemingly never ending questions, and for his teaching efforts. It is highly likely that without the education I received in 2nd year physical chemistry I would have never found the passion towards chemistry, from which I enjoy today.

I would like to thank Dr. David Palmer from Strathclyde university, for taking me in to his group in 2015. The time I spent in Glasgow convinced me to delve deeper in to the world of computational chemistry, and changed the

course of my studies permanently for the better. I would also like to thank Dr. Maksim Misin, Benjamin Smith, and Dr. Samiul Ansari, who helped me immensely when I was taking my first steps in to the world of computational chemistry.

Finally, I would like to thank my family and my comrades. No matter how many rivers I've had to cross, I've never had to go about it on my own.

References

[1] A. Ugrinov and S. C. Sevov. "Rationally Functionalized Deltahedral Zintl Ions: Synthesis and Characterization of $[Ge_9 - ER_3]^{3-}$, $[R_3E - Ge_9 - ER_3]^{2-}$, and $[R_3E - Ge_9 - Ge_9 - ER_3]^{4-}$ $(E = Ge, Sn; R = Me, Ph)$". In: *Chem. Eur. J.* 10 (2004), 3727–3733.

[2] L. Xu and S. C. Sevov. "Oxidative Coupling of Deltahedral Ge_9^{4-} Zintl Ions". In: *J. Am. Chem. Soc.* 121 (1999), 9245–9246.

[3] G. Espinoza-Quintero et al. "Synthesis and Characterization of $[Ru@Ge_{12}]^{3-}$: An Endohedral 3-Connected Cluster". In: *J. Am. Chem. Soc.* 136 (2013), 1210–1213.

[4] J. Joannis. "Action du sodammonium et du potassammonium sur quelques métaux". In: *C. R. Hebd. Seances Acad. Sci.* 113 (1891), 795–798.

[5] S. Scharfe et al. "Zintl Ions, Cage Compounds, and Intermetalloid Clusters of Group 14 and Group 15 Elements." In: *Angew. Chem. Int. Ed.* 50 (2011), 3630–3670.

[6] S. C. Sevov and J. M. Goicoechea. "Chemistry of Deltahedral Zintl Ions". In: *Organometallics* 25 (2006), 5678–5692.

[7] V. Queneau and S. C. Sevov. "Ge_9^{4-}: A Deltahedral Zintl Ion Now Made in the Solid-State". In: *Angew. Chem. Int. Ed.* 36 (1997), 1754–1756.

[8] D. R. Gardner, J. C. Fettinger and B. W. Eichhorn. "Synthesis and Structure of the Metalated Zintl Ion $[Ge_9(\mu_{10} - Ge)Ni(PPh_3]^{2-}$". In: *Angew. Chem. Int. Ed.* 35 (1996), 2852–2854.

[9] A. Ugrinov and S. C. Sevov. "$[Ge_9 = Ge_9 = Ge_9]^{6-}$: A Linear Trimer of 27 Germanium Atoms". In: *J. Am. Chem. Soc.* 124 (2002), 10990–10991.

[10] A. Ugrinov and S. C. Sevov. "$[Ge_9 = Ge_9 = Ge_9 = Ge_9]^{8-}$: A Linear Tetramer of Nine-Atom Germanium Clusters, a Nanorod". In: *Inorg. Chem.* 42 (2003), 5789–5791.

[11] C. Downie, Z. Tang and A. M. Guloy. "An Unprecedented $1_\infty[Ge_9]^{2-}$ Polymer: A Link between Molecular Zintl Clusters and Solid-State Phases". In: *Angew. Chem. Int. Ed.* 39 (2000), 338–349.

[12] A.D. McNaught and A. Wilkinson. *IUPAC. Compendium of Chemical Terminology - 2nd ed. (the "Gold Book")*. Oxford, UK: Blackwell Scientific Publications, 1997.

[13] C. J. Cramer. *Essentials of Computational Chemistry: Theories and Models - 2nd Ed.* Chichester, UK: John Wiley & Sons, Ltd., 2004.

[14] A. R. Leach. *Molecular Modelling: Principles and Applications - 2nd Ed.* Essex, UK: Pearson Education, Ltd., 2001.

[15] A. Szabo and N. S. Ostlund. *Modern Quantum Chemistry: Introduction to Advanced Electronic Structure Theory - Rev. Ed.* Mineola, N.Y.: Dover Publications, 1996.

[16] L. Pauling and E. B. Wilson. *Introduction to Quantum Mechanics With Applications to Chemistry.* Mineola, N.Y.: Dover Publications, 1985.

[17] B. O. Roos and P-O. Widmark. *European Summerschool in Quantum Chemistry 2003, Book I - 3rd Ed.* Lund, Sweden: Lund University, 2003.

[18] P.W. Atkins and R.S. Friedman. *Molecular Quantum Mechanics - 3rd Ed.* Oxford, UK: Oxford University Press, 1997.

[19] J. M. Goicoechea and S.C. Sevov. "Deltahedral Germanium Clusters: Insertion of Transition-Metal Atoms and Addition of Organometallic Fragments". In: *J. Am. Chem. Soc.* 128 (2005), 4155–4161.

[20] J. M. Goicoechea and S.C. Sevov. "$[(Ni-Ni-Ni)@(Ge_9)_2^{4-}]$: A Linear Triatomic Nickel Filament Enclosed in a Dimer of Nine-Atom Germanium Clusters". In: *Angew. Chem. Int. Ed.* 44 (2005), 4026–4028.

[21] M. J. Frisch et al. *Gaussian09, Revision E.01.* Gaussian Inc. Wallingford CT 2009.

[22] A. D. Becke. "Density-functional thermochemistry. III. The role of exact exchange". In: *J. Chem. Phys.* 98 (1993), 5648–5652.

[23] B. Miehlich et al. "Results obtained with the correlation-energy density functionals of Becke and Lee, Yang and Parr". In: *Chem. Phys. Lett.* 157 (1989), 200–206.

[24] C. Lee, W. Yang and R. G. Parr. "Developement of the Colle-Salvetti correlation-energy formula into a functional of the electron density". In: *Phys. Rev. B* 37 (1988), 785–789.

[25] Francesco Aquilante et al. “Molcas 8: New capabilities for multiconfigurational quantum chemical calculations across the periodic table”. In: *J. Comp. Chem.* 37 (2016), 506–541.